Comparison Between Multiline Transmission and Diverging Wave Imaging: Assessment of Image Quality and Motion Estimation Accuracy

Emilia Badescu, Damien Garcia, Philippe Joos, Adeline Bernard, Lionel Augeul, René Ferrera, Magalie Viallon, Lorena Petrusca, Denis Friboulet, and Hervé Liebgott

***Abstract*— High frame rate imaging is particularly important in echocardiography for better assessment of the cardiac function. Several studies showed that diverging wave imaging (DWI) and multiline transmission (MLT) are promising methods for achieving a high temporal resolution. The aim of this study was to compare MLT and compounded motion compensation (MoCo) DWI for the same transmitted power, same frame rates [image quality and speckle tracking echocardiography (STE) assessment], and same packet size [tissue Doppler imaging (TDI) assessment]. Our results on static images showed that MLT outperforms DW in terms of resolution (by 30% on average). However, in terms of contrast, MLT outperforms DW only for the depth of 11 cm (by 40% on average), the result being reversed at a depth of 4 cm (by 27% on average). *In vitro* results on a spinning phantom at nine different velocities showed that similar STE axial errors (up to 2.3% difference in median errors and up to 2.1% difference in the interquartile ranges) are obtained with both ultrafast methods. On the other hand, the median lateral STE estimates were up to 13% more accurate with DW than with MLT. On the contrary, the accuracy of TDI was only up to ∼3% better with MLT, but the achievable DW Doppler frame rate was up to 20 times higher. However, our overall results showed that the choice of one method relative to the other is therefore dependent on the application. More precisely, in terms of image quality, DW is more suitable for imaging structures at low depths, while MLT can provide an improved image quality at the focal point that can be placed at higher depths. In terms of motion estimation, DW is more suitable for color Doppler-related applications, while MLT could be used to estimate velocities along selected lines of the image.**

***Index Terms*— Diverging waves (DWs), multiline transmission (MLT), speckle tracking, tissue Doppler imaging (TDI), ultrafast imaging.**

Manuscript received March 21, 2019; accepted June 22, 2019. Date of publication June 27, 2019; date of current version September 25, 2019. This work was supported in part by the European Union's Horizon 2020 Research and Innovation Programme [VPH-CaSE (www.vph-case.eu)] under Marie Skłodowska-Curie Grant 642612 and in part by Laboratoire d'Excellence (LABEX) Centre Lyonnais d'Acoustique (CELYA) (ANR-10-LABX-0060). *(Corresponding author: Emilia Badescu.)*

E. Badescu, D. Garcia, P. Joos, A. Bernard, D. Friboulet, and H. Liebgott are with Université Lyon, INSA-Lyon, Université Claude Bernard Lyon 1, UJM-Saint Etienne, CNRS, Inserm, CREATIS UMR 5220, U1206, 69100 Villeurbanne, France (e-mail: emilia.badescu.@yahoo.com).

L. Augeul and R. Ferrera are with the CarMeN Laboratory, Université Lyon, INSERM, INRA, INSA Lyon, Université Claude Bernard Lyon 1, 69600 Villeurbanne, France.

M. Viallon and L. Petrusca are with Université Lyon, UJM-Saint-Etienne, INSA, CNRS UMR 5520, INSERM U1206, CREATIS, 42023 Saint-Étienne, France.

Digital Object Identifier 10.1109/TUFFC.2019.2925581

I. Introduction

THE advantages of echocardiography over other imaging modalities in terms of acquisition time, cost, and noninvasiveness justify its common usage in daily clinical practice. Although good clinical results were reported when using the frame rate achievable in standard echocardiography (∼40–80 Hz), heart dynamics contains short events that cannot be captured with the conventional frame rate. Higher temporal resolution might be essential in rapid cardiac events observed in a number of cases such as stress echocardiography, fetal echocardiography, multichamber motion/strain imaging, or intracavitary blood flow dynamics [1]. In response to the need for higher frame rates, several methods have been proposed in ultrasound imaging. The concept of ultrafast echographic imaging was introduced four decades ago by Bruneel *et al.* [2], and this methodology evolved in parallel with the technological progress. Conventionally, an increase in the frame rate could be achieved by reducing the line density and/or the sector size, but with the trade-off of resolution loss and field-of-view limitation. To overcome this compromise, a processing method based on reconstructing multiple image lines from one single transmission has been proposed by Shattuck *et al.* [3]. This method is commonly referred to as multiline acquisition (MLA) and it is implemented in most current clinical scanners [1]. An alternative technique based on a time reversal approach was introduced by Fink [4]. Other approaches proposed combined images of several subsectors acquired individually at a high frame rate using retrospective electrocardiogram (ECG) gating [5]. A better gain in temporal resolution became possible with the emergence of ultrafast methods which can use both unfocused and focused beams. The unfocused beam approaches use a subaperture to simulate a virtual point located behind the probe. While the first investigations of this approach were referred to as synthetic aperture multielement techniques [6], later contributions are known as plane wave (PW) [7] or diverging wave (DW) [8] techniques. As an alternative, the frame rate can be increased using focused beam approaches like multiline transmission (MLT) [9]. The achieved high frame rates led to innovative quantitative tools in echocardiography, such as the assessment of electromechanical properties of the heart [10], solving the incompatibility between imaging and

quantification for blood flow characterization [11], [12], and the evaluation of 2-D vector flow dynamics within the same cardiac cycle [13].

Compared with the conventional single line transmit (SLT) imaging, where one focused transmission is needed for each line of the image, the MLT principle is based on transmitting n focused beams simultaneously, thus allowing an n-fold increase in the frame rate. Several studies based on both simulations [14] and *in vivo* acquisitions [15] showed the potential of this method for achieving high frame rates while mostly preserving image quality. Additionally, it has been shown that MLT can be efficiently combined with MLA to further improve the temporal resolution. Although the increase in temporal resolution does not compromise to a great extent the contrast, resolution, and signal-to-noise ratio (SNR) compared to SLT, it does compromise the amount of image artifacts as a result of simultaneous transmissions. Since MLT is prone to crosstalk, many studies focused on reducing the image artifacts [14], [16], [17]. Although tissue Doppler imaging (TDI) has been applied to MLT images [18], [19], this beamforming method has received little attention in motion estimation.

Alternative ultrafast methods using plane or DWs allow one to obtain an entire image with a single transmission. Since the time needed for insonifying a full image by using plane/DW imaging (DWI) corresponds to the time needed for insonifying n lines of the image with MLT and one single line with SLT, the frame rate is considerably increased. Image quality is, however, significantly compromised in terms of both resolution and contrast [20]. Coherent compounding has thus been proposed to cope with this limitation [6], [12], [20]. By coherently summing multiple images obtained at different PW/DW obliquities, image quality can be improved substantially. Since this approach may fail if the medium is characterized by a strong motion from one transmission to another, motion compensation (MoCo) can be used in the presence of high-velocity tissues to ensure adequate coherent compounding. MoCo was first introduced in synthetic aperture imaging for axial MoCo [21] and later extended to 2-D MoCo approaches [22]. The potential of MoCo has been shown *in vivo* for abdominal imaging using synthetic aperture approaches [23] and for cardiac imaging using TDI DW approaches [24]. Recently, the importance of using DW MoCo has been demonstrated in improving the speckle tracking echocardiography (STE) accuracy [25]. Furthermore, other studies showed that coupling optical flow and TDI methods for STE could provide more precise velocity vector estimates in the in-range direction [26].

In this study, we proposed a comparison between two promising ultrafast methods (DWI with MoCo and MLT imaging) in terms of image quality, motion artifacts, and their effects on motion estimation using speckle tracking and TDI. To our knowledge, this is the first such comparison proposed in the literature.

II. Methods

A. Acquisition Set-Up

The data were acquired with a Verasonics research scanner (Verasonics, Inc., Redmond, WA, USA) and a P4-2 phased array probe having 64 elements and a central frequency of 2.5 MHz. The pulse repetition frequency (PRF) was set to 4500 Hz, the sector size to 90°, and the maximum range to 13 cm.

There are different ways to compare two methods in a fair way. In this study, as a general principle, we have chosen to adopt the transmission waveform in order to obtain the same total emitted power for both MLT and DW. For MLT, we used an excitation signal which was on during 1/5 of the half cycle and off for the rest of the time. We computed the transmission matrix by overlapping the excitation signals corresponding to all elements and all simultaneous transmissions. Then, we compared the resulting signals with a threshold in order to obtain a tristate pulse ($-1/0/+1$), as required by the Verasonics system. The transmitted signal, and consequently the transmitted power for MLT was different for each transmission and for each element. However, the total transmitted power calculated over all elements and over all transmissions did not change considerably when the frame rate was varied (the frame rate values will be presented further in Sections II-B and II-C for speckle tracking and Doppler acquisitions, respectively). This was because, at a low frame rate, the low power that resulted from a reduced superposition of waveforms in a single transmit-event was compensated by summing the power over many transmissions. On the other hand, at a high frame rate, the high power that resulted from a high superposition of waveforms in a single transmit-event was compensated by summing the power over less transmissions. But for DW, the total transmitted power decreased with the number of transmissions, since the power in a single event transmission was constant. Therefore, the total transmitted power with MLT did not vary much with the decrease of the frame rate as it did for DW. We compensated for that by modifying the transmit waveforms when using a reduced number of steering angles for DW. Details on how the excitation signals were changed for DW and how the power was balanced for static/STE acquisitions, on one hand, and for Doppler acquisitions, on the other hand, are provided in Sections II-B and II-C, respectively.

The simulated acoustic pressure field obtained with the two methods for one transmission is represented in Fig. 1.

B. Acquisition Settings for Image Quality Assessment and Speckle Tracking Motion Estimator

Same frame rates were used for static conditions and speckle tracking. More specifically, the tested frame rates were set to 225, 450, and 900 Hz by reducing the number of transmission events per reconstructed image from 20 to 10 and to 5. An overview of the transmission setting applied to DW and MLT for obtaining the same frame rates is presented in Table I.

The total power of the two high frame-rate methods was balanced using in the following equation:

$$P_{\mathrm{MLT/DW}}^{\mathrm{BS}} = \sum_{t=1}^{N_{\mathrm{tx}}} \sum_{e=1}^{N_e} \frac{1}{N_s} \sum_{s=1}^{N_s} |\mathrm{wf}_{\mathrm{set}}|^2 \tag{1}$$

where $\mathrm{wf}_{\mathrm{set}}$ represents one sample s of the waveform wf applied to the element e of the transducer for the transmission

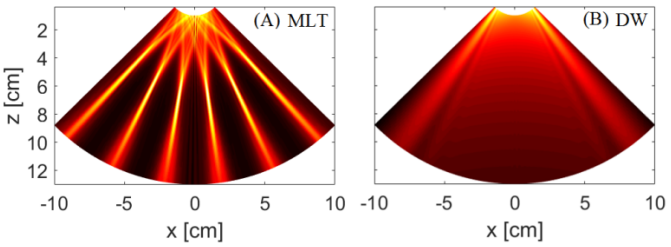

Fig. 1. Pressure field obtained for one transmission with (a) MLT and (b) DW. Results obtained using an in-house simulation tool.

TABLE I
TRANSMISSION SETTINGS MLT VERSUS DW

Frame Rate	Number of Transmit events	MLT: number of simultaneous transmissions	DW: number of tilt angles
225 Hz	20	3	20
450 Hz	10	6	10
900 Hz	5	12	5

t; N_s is the number of samples of the waveform wf, N_e is the number of elements of the transducer, and N_{tx} is the total number of transmissions needed to form an image (MLT) or a compound image (DW). This equation holds for both B-mode and STE acquisitions (notation: BS).

Once the power was calculated for each frame rate in MLT, the duty cycle (given by the ratio between the pulse active time and the total period of the pulse) of the transmitted DW waveform was modified to match the same total power for each of the three settings. Since the length of the signals was constant (the only changing parameter was the duty cycle), the transmit waveform had half of a cycle for both modalities.

1) Diverging Waves: The maximum tilt angle was varied with the number of transmissions. Therefore, for the lowest frame rate of 225 Hz, we used the range $[-8.6°, 8.6°]$; for the frame rate of 450 Hz, we used the range $[-4.3°, 4.3°]$; and for the highest frame rate of 900 Hz, the maximum tilt angle was $\pm 2.15°$. The resulting lateral (x) position ranges of the virtual sources obtained using these tilt angles were: $[-2.98, 2.98]$ mm for 20 DW, $[-1.51, 1.51]$ mm for 10 DW, and $[-0.75, 0.75]$ mm for 5 DW. Since small maximum tilt angles were employed for all three settings, the axial (z) position of the virtual sources slightly changed from -10 mm (tilt angles up to $\pm 4.3°$) to -9.6 mm (tilt angle $\pm 8.6°$). Using a constant angular pitch ensures avoiding transmit grating lobes.

The position of the side lobes changes with the variation of the tilt angles. Even under static conditions, MoCo detects the modification of the side lobes position as a movement. When the tilt angles are linearly increasing, this method rephases the side lobes to the same position. By arranging the tilt angles in a triangular sequence, the side lobes can be rephased along two different directions which helps in reducing the side lobe effect [24].

MoCo compensates for the radial motion using the slow time autocorrelation on M successive received IQ signals. The phase angle (ϕ_{MoCo}), giving the phase delays due to motion, was calculated using the product of the two autocorrelations (R_1, R_2) corresponding to the ascending and the descending parts of the triangular sequence. As shown in (2), a 1/2 factor is needed to recover the phase angle, which decreases the maximum detectable velocity by a factor 2, compared to the Nyquist velocity

$$\phi_{\text{MoCo}}(\theta, r) = \frac{1}{2}\arg\{R_1 R_2\} \tag{2}$$

where (θ, r) are the polar coordinates and arg represents the argument of the complex $R_1 R_2$.

The image quality and motion estimation were evaluated on compounded MoCo B-Mode images using the triangular sequence.

2) Multiline Transmit: For achieving equivalent temporal resolution, we progressively increased the number of simultaneous transmissions to 3, 6, and 12. The focal point was set to 7 cm. No apodization was used to transmit or receive. Image reconstruction was performed using 5 MLA, meaning that five image lines centered in the focal point of the transmitted beam were reconstructed in parallel.

TABLE II
TDI TRANSMISSION SETTINGS MLT VERSUS DW

Packet size	MLT		DW	
	Number of simultaneous transmissions	Frame Rate	Number of tilt angles	Frame Rate
8	3	28 Hz	8	562 Hz
8	6	56 Hz	8	562 Hz
8	12	112 Hz	8	562 Hz

C. Acquisition Settings for Tissue Doppler Imaging

We fixed constant the two parameters having a high impact on the estimator for both MLT and DW: the PRF and the packet size. Since for DW, the compounding was computed in parallel with the Doppler estimator, the packet size corresponds to the number of tilt angles. Given the PRF of 4500 Hz and a packet size of 8, the resulting Doppler frame rate is 562 Hz. To study the effect of crosstalk in MLT, we kept the same simultaneous focused transmission configurations as for speckle tracking: 3 MLT, 6 MLT, and 12 MLT. However, since we needed to steer eight times on the same place for each transmission, the Doppler frame rate was drastically decreased to 28, 56, and 112 Hz. An overview of these parameters is presented in Table II.

For Doppler acquisitions, the total power was calculated and balanced using (3) for MLT and (4) for DW

$$P_{\text{MLT}}^{\text{TDI}} = \text{PS} \cdot \sum_{t=1}^{N_{\text{tx}}} \sum_{e=1}^{N_e} \frac{1}{N_s} \sum_{s=1}^{N_s} |\text{wf}_{\text{set}}|^2 \tag{3}$$

$$P_{\text{DW}}^{\text{TDI}} = \text{PS} \cdot \sum_{e=1}^{N_e} \frac{1}{N_s} \sum_{s=1}^{N_s} |\text{wf}_{\text{set}}|^2 \tag{4}$$

where PS is the packet size. We found it necessary to use the number of transmissions needed to form a full MLT image since a 2-D autocorrelation was used for Doppler estimation. Therefore, the total power obtained with MLT was much higher than that obtained with DW using half-cycle waveforms. Adapting just the duty cycle was not enough to balance the two total powers. Thus, we needed to use longer waveforms for DW: between 1 and 1.5 cycles for TDI acquisitions, depending on the number of transmissions. Although this allows balancing the total transmitted power, one could expect a direct impact of the pulselength on the TDI performance.

D. In Vitro Models

1) Image Quality Assessment on Static Phantoms: The image quality was first evaluated on a Gammex phantom using contrast and resolution metrics as proposed in [27]. Therefore, we used as a metric the contrast to noise ratio (CNR) defined as

$$\mathrm{CNR} = 20\log_{10}\left(\frac{\left|\mu_{\mathrm{bck}} - \mu_{\mathrm{cyst}}\right|}{\sqrt{\sigma^2_{\mathrm{bck}} + \sigma^2_{\mathrm{cyst}}}}\right) \tag{5}$$

where μ_{bck}, μ_{cyst} are the means and σ^2_{bck}, σ^2_{cyst} are the corresponding variances of the background and the cyst regions calculated for a B-Mode image.

We evaluated the contrast at 4 and 11 cm, respectively, for the three settings mentioned in Table I. Our dynamic range was 60 dB.

For the same acquisition settings, the resolution was evaluated at four different image depths (from 5 to 11 cm with a step of 2 cm) using the full width at half maximum (FWHM).

2) Image Quality Assessment on Dynamic Phantoms: The image quality assessment under dynamic conditions was performed on a tissue mimicking rotating disc phantom made from agar (4%), silica (1%), and water. The disc was created to contain four inclusions for facilitating the contrast assessment. The CNR was computed using the mean of the four inclusions for each frame. The velocity of the disc was controlled by a step motor and adjusted to nine different values from 50°/s to 450°/s, using a step of 50°.

For each velocity, the mean CNR for the four inclusions was averaged over ten frames.

E. In Vivo Models

In vivo data were acquired in an open-chest pig. The experiments were approved by the Animal Ethics Committee with agreement number A693830501. Parasternal short axis views were examined for both B-mode images and tissue Doppler. The acquisition sequences and settings were similar to those used for the *in vitro* data. The only difference was the focal point for MLT which was placed at 4 cm, due to the available view. The DW and MLT acquisition sequences were concatenated, and the buffers were adapted to receive alternatively sets of DW and MLT frames. Thus, the comparison could be assessed at close cardiac phases within the same cardiac cycle. For B-mode images, an intermediate frame rate of 450 Hz was chosen for both DW and MLT (Table I, third row; the heading is considered as the first row). Similarly, the intermediate settings provided in Table II (third row; heading is considered as the first row) were used for *in vivo* TDI acquisitions.

F. Motion Estimation Methods

The influence of the two ultrafast imaging strategies on motion estimation was tested using speckle tracking and tissue Doppler (TDI).

A block matching STE method was used based on the normalized cross correlation in the Fourier domain [28]. The B-Mode images were divided into 32 × 32 windows. The speckles were tracked with a window overlap of 50%. The pixel size was 0.28 mm in the radial direction and 0.3° in the cross range direction. For achieving a subpixel precision, parabolic peak fitting was applied to the estimator. Since we used high frame rate imaging, it seemed legitimate to assume constant motion between successive frames. Therefore, to improve the robustness of the method, we used an ensemble correlation over 15 frames. The frame lag was increased from 1 to 2 and 4 for the frame rates of 225, 450, and 900 Hz since it is known that block matching is better adapted to extract displacements greater than one pixel. The speckle tracking parameters (window size, frame lag) were chosen to obtain good estimates when applied to DW images. Then, the same parameters were used for MLT images. Since the two high temporal resolution imaging methods (MLT and DW) were compared at the same frame rates and on images having the same pixel size and number of pixels, choosing the same parameters (frame lag and window size) should provide equivalent conditions for the two methods.

Doppler velocity was estimated using a 2-D auto-correlator applied on the IQ data, as proposed in [29] and [30]. By using this method, the phase shift was used to estimate the displacement. In order to retain a high Doppler frame rate, TDI was applied to uncompounded DW images. With a PRF of 4500 Hz, the maximum velocity that we could detect with no aliasing was 69 cm/s with MLT and 35 cm/s for DW MoCo (2).

The accuracy of the estimates in a selected direction d was evaluated using the absolute deviation error (ADE) for each pixel i, given byX

$$\mathrm{ADE}_{di} = \frac{|V_{\mathrm{ref}_{di}} - V_{\mathrm{estim}_{di}}|}{|V_{\mathrm{ref}_d}|_{\max}} \tag{6}$$

where $V_{\mathrm{ref}_{di}}$ and $V_{\mathrm{estim}_{di}}$ are the reference and estimated velocities for a given pixel i and in a selected direction d ($d = x$ for lateral; $d = z$ for axial); $\left|V_{\mathrm{ref}_d}\right|_{\max}$ is the maximum of the absolute reference velocities over the entire image.

III. Results

A. Image Quality Assessment on Static Phantoms

Fig. 2 shows the B-Mode images of the Gammex phantom obtained at different frame rates. The left column illustrates the results of using an MLT transmission, whereas the right

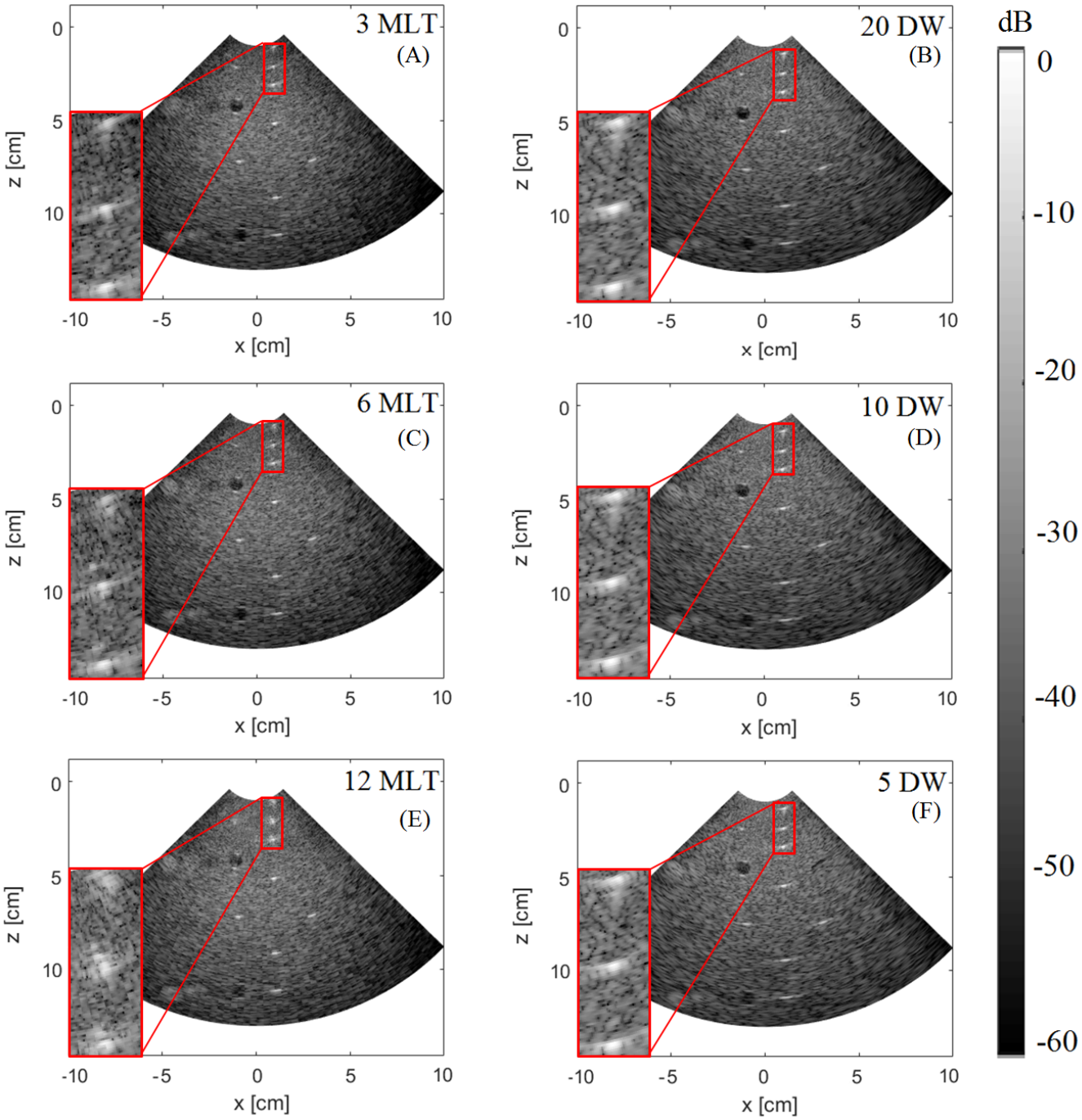

Fig. 2. Image quality of MLT (left column) and DW (right column) by using a frame rate of (a) and (b) 225 Hz, (c) and (d) 450 Hz, and (e) and (f) 900 Hz. A zoomed-in view (x = [0.4 cm:1.4 cm]; z = [0.8 cm:3.5 cm]) is provided in the red box for (a), (c), and (e) MLT in comparison with (b), (d), and (f) DW for better visualization of artifacts next to the surface of the probe.

column corresponds to the images resulting from compounded DW. For facilitating the comparison, each row of Fig. 2 displays images acquired at different frame rates.

The contrast values (CNR) for a hypoechoic cyst at 4 cm is reported in Table III and for a cyst at 11 cm in Table IV.

The lateral resolution (FWHM) at four different image depths (5, 7, 9, and 11 cm) is illustrated in Table V, for all three frame rates. However, the resolution did not change significantly from 5 to 10 or 20 DWs. The same trend of lateral resolution saturation starting with a limited number of DWs was also reported in other studies [31].

B. Image Quality Assessment on the Rotating Disc Phantom

In order to observe how the contrast is affected by images undergoing motion, we calculated the CNR for nine different velocities of the disc. The results are illustrated in Fig. 3. For each velocity, we plotted the mean contrast over ten frames and the corresponding standard deviation.

C. Motion Estimation Accuracy

Fig. 4 shows the axial (in-range) error distribution, while Fig. 5 shows the lateral (cross-range) error distribution using

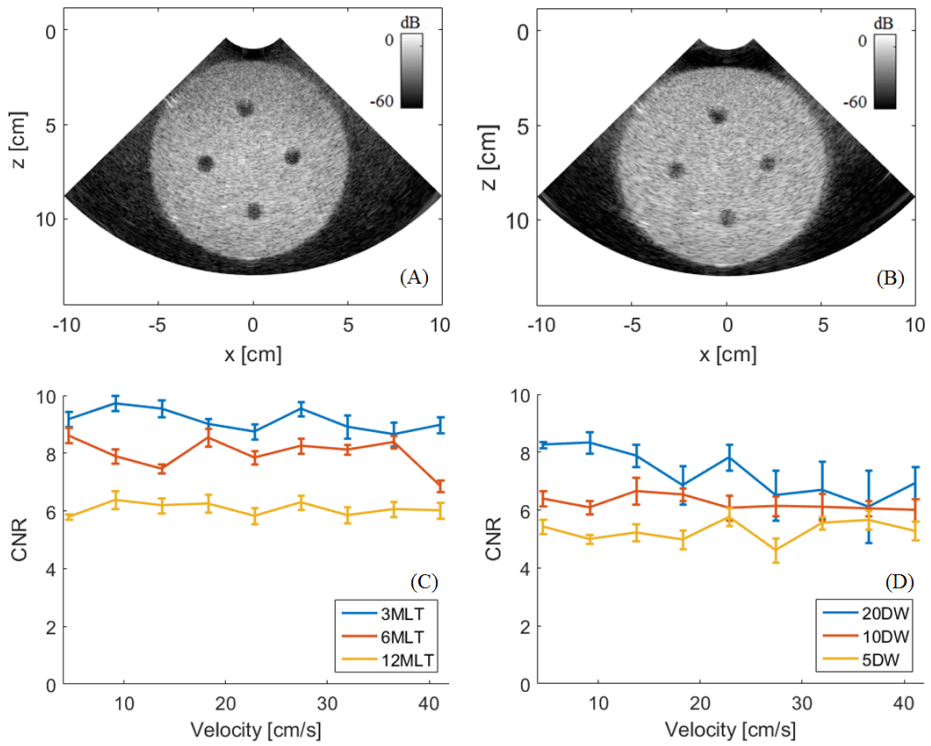

Fig. 3. CNR at different velocities of the disc calculated on the phantom shown (for qualitative evaluation) in (a) for MLT and in (b) for DW. Results of (c) MLT and (d) DW at frame rates of 225 Hz (blue), 450 Hz (red), and 900 Hz (yellow).

TABLE III
CNR VALUES FOR CYST AT 4 cm

Frame rate/ Transmission Type	225 Hz	450 Hz	900 Hz
MLT	6.38 dB	5.66 dB	3.75 dB
DW	8.82 dB	7.54 dB	5.36 dB

TABLE IV
CNR VALUES FOR CYST AT 11 cm

Frame rate/ Transmission Type	225 Hz	450 Hz	900 Hz
MLT	5.35 dB	4.46 dB	1.51 dB
DW	4.84 dB	3.53 dB	0.12 dB

speckle tracking. The median of the ADE is represented in red, while the lower and upper box limits are the first and third quartiles of the error. The results obtained with MLT (left) and DW (right) at different frame rates are illustrated: 225 Hz (a) and (b), 450 Hz (c) and (d), 900 Hz (e) and (f). Similarly, Fig. 6 shows the TDI results obtained with MLT (left) and DW (right) for the same packet size of 8 and a different number of simultaneous transmissions: (a), (c), and (e). Below each set of boxplot, we show the differences in median (*Med*) and interquartile range (IQR) between MLT and DW. The IQR was calculated by subtracting the 25th percentile from the 75th percentile of the ADE. In order to study if the medians and IQRs obtained with the two methods are statistically different, we used a two-sided Wilcoxon rank sum test between the two groups (MLT and DW) containing nine samples each (one for each velocity). The last column from each table shows if the resulting p-value allows rejecting the null hypothesis at 5% significance level.

D. Qualitative B-Mode and TDI In Vivo Assessment

In Fig. 7, we show B-mode images obtained at the intermediate frame rate of 450 Hz for both MLT (a) and DW (b). Additionally, we show in Fig. 8 the tissue Doppler images for the two high frame rate methods. Two pairs of TDI images are shown at two different phases of the cardiac cycles. MLT and DW TDI results are first shown during ventricular filling when the mitral valve is fully opened (a) and (b) and second the same images are shown when the mitral valve starts to close (c) and (d).

IV. DISCUSSION

A. Image Quality Assessment: Phantom Experiments

Fig. 2 shows the image quality degradation with the decrease in the number of transmissions, and therefore the increase in the frame rate. Even if the degradation was present for both MLT and DW, its nature was different for the two methods. For instance, for MLT, the amount of crosstalk artifacts at a depth of up to 4 cm was considerably increased as seen in magnified regions marked by the red boxes of Fig. 2(a), (c), and (e). On the other hand, using DW led to a good image quality up to 4 cm. In addition to the absence of crosstalk, the CNR of the cyst placed at 4 cm was higher for the DW wide beam transmission as compared to the focused beam transmission (Table III). However, DW showed a higher

TABLE V
LATERAL RESOLUTION AT DIFFERENT IMAGE DEPTHS FOR THE FRAME RATES OF 225, 450, AND 900 Hz

Trans-mission Type	Frame rate	225 Hz				450 Hz				900 Hz			
	Depth of the inclusion	5 cm	7 cm	9 cm	11 cm	5 cm	7 cm	9 cm	11 cm	5 cm	7 cm	9cm	11cm
MLT	FWHM	1.6 mm	1.9 mm	2.2 mm	3.6 mm	1.7 mm	1.9 mm	2.2 mm	3.6 mm	1.7 mm	1.9 mm	2.2 mm	3.6 mm
DW		2.1 mm	3.3 mm	3.6 mm	4.5 mm	2.2 mm	3.3 mm	3.6 mm	4.5 mm	2.2 mm	3.3 mm	3.6 mm	4.5 mm

attenuation of the signal at higher depths compared to MLT for all frame rates (although the transmitted energy was equivalent for the two methods). This explains the CNR values for the cyst at 11 cm that were reduced when the unfocused DW transmission was used compared to MLT (Table IV). This phenomenon appears even though the position of the cyst at 11 cm is 4 cm away from the focal point.

We evaluated the lateral resolution starting from 5 to 11 cm with a step of 2 cm. Our results (Table V) showed that similar FWHM values are obtained for the same depth and at a different frame rate, which is consistent with other studies from the literature, showing that the lateral resolution improves quickly with the number of DWs [31]. Moreover, for all settings considered, we were above 3 DWs, which is the value required for stabilizing the lateral resolution. As it can be observed in Table V, a better resolution was achieved by using MLT than by using DW, and the resolution degraded with depth for both methods. However, the lateral resolution with DWI could be improved further by using a higher angular pitch.

The qualitative contrast evaluation on the rotating disc phantom shown in Fig. 3(a) and (b) indicates the trend of MLT to offer a better contrast for the inclusions close to the focal point and the trend of DW to offer a better contrast at low depths. The quantitative assessment over all inclusions showed the degradation of the contrast with the increase of the temporal resolution for all the velocities applied to the motor [Fig. 3(c) and (d)]. Note that the higher CNR values obtained in the rotating disc phantom compared with the Gammex phantom came from the difference in echogenicity between the two phantoms. The CNR was approximatively constant with the variation of the velocity, which is consistent with the results presented in [24]. However, the curves present slight deviations which appeared as a consequence of calculating the average CNR at different positions of the inclusions at different velocities. Despite this limitation, the trend of a better MLT contrast compared to DW MoCo can still be observed for all velocities and for all frame rates. This can be explained by the fact that the cysts were placed from 4.5 to 9.5 cm in a region of interest, where we showed that MLT is likely to be more accurate. Evaluating the CNR under dynamic conditions at lower penetration depths may lead to opposite results since the MLT crosstalk level is increased at low depths.

B. Motion Estimation Assessment: Phantom Experiments

When speckle tracking was applied to MLT images and compounded motion-compensated DW images, similar medians and IQR values were obtained in both cases in the axial direction for each frame rate and velocity value (Fig. 4). For all the acquisitions, the difference in median and IQR was inferior to 2.3%. The predominant negative values for the frame rates of 225 and 450 Hz show the trend of MLT to perform slightly better than DW, which can be associated with the impact of focusing on the B-Mode image quality. On the other hand, this trend is less general for the frame rate of 900 Hz, where the presence of transmit artifacts in MLT is more significant. Despite the small differences (less than 2.3%) in medians for the frame rates of 225 and 450 Hz, the p-value shows that the two methods provide statistically different medians of error. This can be explained by the fact that each median is calculated over a very large number of samples ($\sim 10^7$), resulting in narrow and nonoverlapping distributions of each two groups tested.

The difference in the results obtained with the two methods is larger in the lateral direction, especially in terms of IQR, going up to 17.7% (Fig. 5). The p-values reported in Fig. 5 show that the difference in results between the two methods is statistically significant for all frame rates and for both IQR and medians. The lower performance of MLT can be associated with the discontinuities between the lines of the images found on the B-Mode images. The image appearance looks smoothed in DW compared to MLT due to the compounding process. Additionally, the lateral performance could be improved by reducing the crosstalk level as suggested in [15]. For both directions and all frame rates considered, we can observe the trend of the block matching to provide less accurate estimates at the lowest velocity (reduced movement between the frames). Since we compensated for a higher temporal resolution by incrementing the lag between the frames, the estimator is not significantly affected by the frame rate variation.

When TDI was investigated for the two high-frame rate methods, the predominant negative difference in medians and IQR indicates slightly better estimates for MLT (Fig. 6). However, the improvement was inferior to 3% for all the cases. On the other hand, DW allows performing compounding and MoCo for B-Mode visualization based on the same packet size used for motion estimation. Thus, the temporal resolution is diminished just by a single parameter: the packet size. On the contrary, for estimating the Doppler velocities on MLT images while preserving a high PRF, successive transmissions have to be performed several times for the same image location. Therefore, the time required between the formation of the first and the last line of the image is increased not only with the packet size but also with the number of transmissions needed to achieve a full B-Mode image. In consequence,

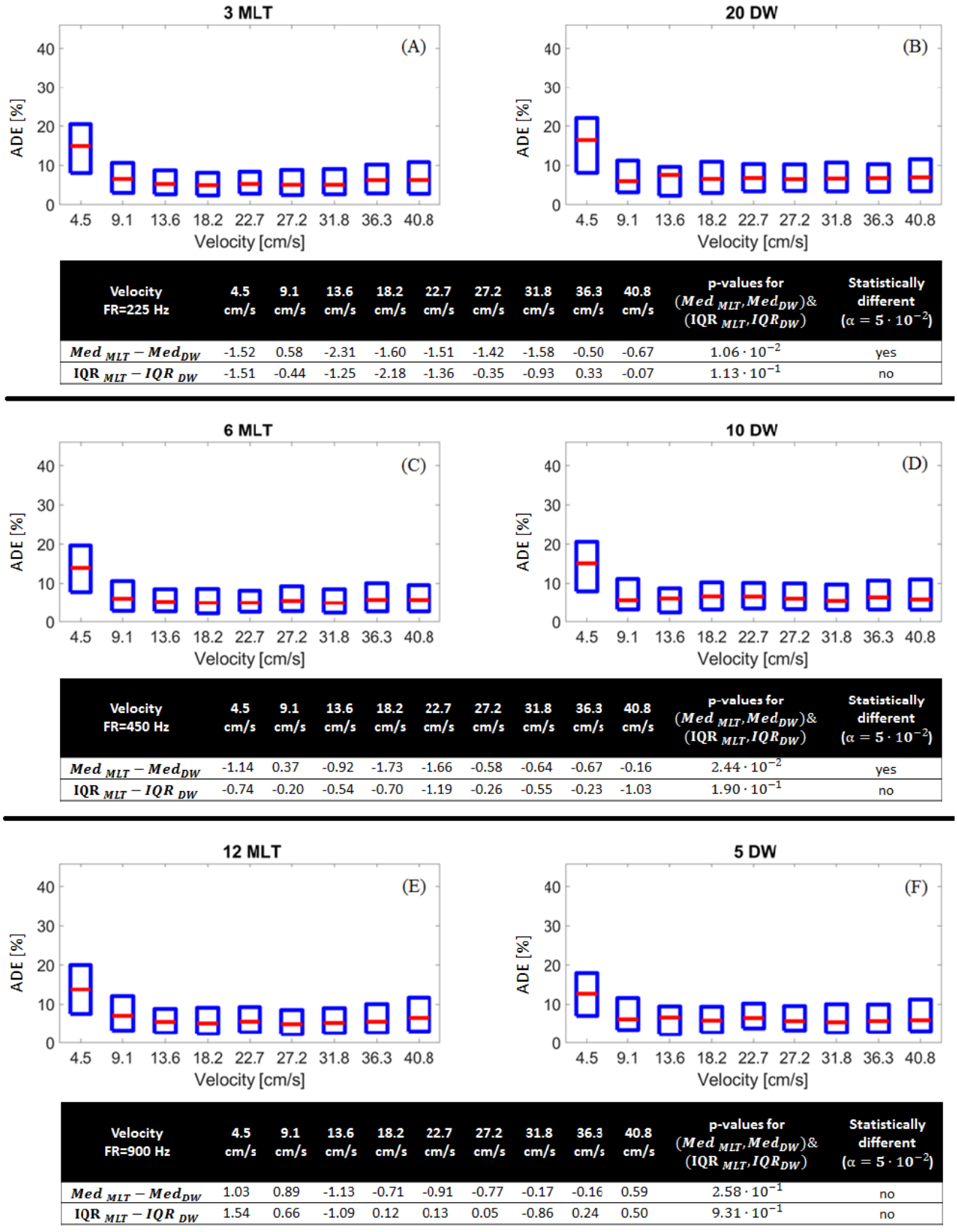

Velocity FR=225 Hz	4.5 cm/s	9.1 cm/s	13.6 cm/s	18.2 cm/s	22.7 cm/s	27.2 cm/s	31.8 cm/s	36.3 cm/s	40.8 cm/s	p-values for (Med_{MLT}, Med_{DW})& (IQR_{MLT}, IQR_{DW})	Statistically different ($\alpha = 5 \cdot 10^{-2}$)
$Med_{MLT} - Med_{DW}$	-1.52	0.58	-2.31	-1.60	-1.51	-1.42	-1.58	-0.50	-0.67	$1.06 \cdot 10^{-2}$	yes
$IQR_{MLT} - IQR_{DW}$	-1.51	-0.44	-1.25	-2.18	-1.36	-0.35	-0.93	0.33	-0.07	$1.13 \cdot 10^{-1}$	no

Velocity FR=450 Hz	4.5 cm/s	9.1 cm/s	13.6 cm/s	18.2 cm/s	22.7 cm/s	27.2 cm/s	31.8 cm/s	36.3 cm/s	40.8 cm/s	p-values for (Med_{MLT}, Med_{DW})& (IQR_{MLT}, IQR_{DW})	Statistically different ($\alpha = 5 \cdot 10^{-2}$)
$Med_{MLT} - Med_{DW}$	-1.14	0.37	-0.92	-1.73	-1.66	-0.58	-0.64	-0.67	-0.16	$2.44 \cdot 10^{-2}$	yes
$IQR_{MLT} - IQR_{DW}$	-0.74	-0.20	-0.54	-0.70	-1.19	-0.26	-0.55	-0.23	-1.03	$1.90 \cdot 10^{-1}$	no

Velocity FR=900 Hz	4.5 cm/s	9.1 cm/s	13.6 cm/s	18.2 cm/s	22.7 cm/s	27.2 cm/s	31.8 cm/s	36.3 cm/s	40.8 cm/s	p-values for (Med_{MLT}, Med_{DW})& (IQR_{MLT}, IQR_{DW})	Statistically different ($\alpha = 5 \cdot 10^{-2}$)
$Med_{MLT} - Med_{DW}$	1.03	0.89	-1.13	-0.71	-0.91	-0.77	-0.17	-0.16	0.59	$2.58 \cdot 10^{-1}$	no
$IQR_{MLT} - IQR_{DW}$	1.54	0.66	-1.09	0.12	0.13	0.05	-0.86	0.24	0.50	$9.31 \cdot 10^{-1}$	no

Fig. 4. *Axial* ADE at different velocities of the disc at different frame rates (*Speckle Tracking*): (a) and (b) 225 Hz, (c) and (d) 450 Hz, and (e) and (f) 900 Hz. Below each set of boxplot, we show the differences in median (*Med*) and IQR between MLT and DW. Additionally, we provide the associated *p*-values.

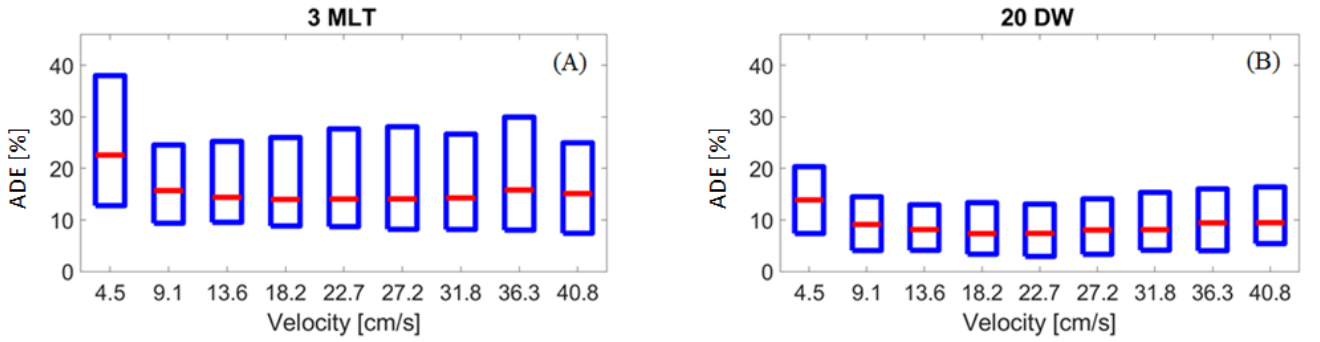

Velocity FR=225 Hz	4.5 cm/s	9.1 cm/s	13.6 cm/s	18.2 cm/s	22.7 cm/s	27.2 cm/s	31.8 cm/s	36.3 cm/s	40.8 cm/s	p-values for (Med_{MLT}, Med_{DW}) & (IQR_{MLT}, IQR_{DW})	Statistically different ($\alpha = 5 \cdot 10^{-2}$)
$Med_{MLT} - Med_{DW}$	8.69	6.57	6.23	6.62	6.66	6.04	6.15	6.36	5.63	$4.11 \cdot 10^{-5}$	yes
$IQR_{MLT} - IQR_{DW}$	12.23	4.73	6.84	7.15	8.79	9.12	7.27	9.91	6.54	$4.11 \cdot 10^{-5}$	yes

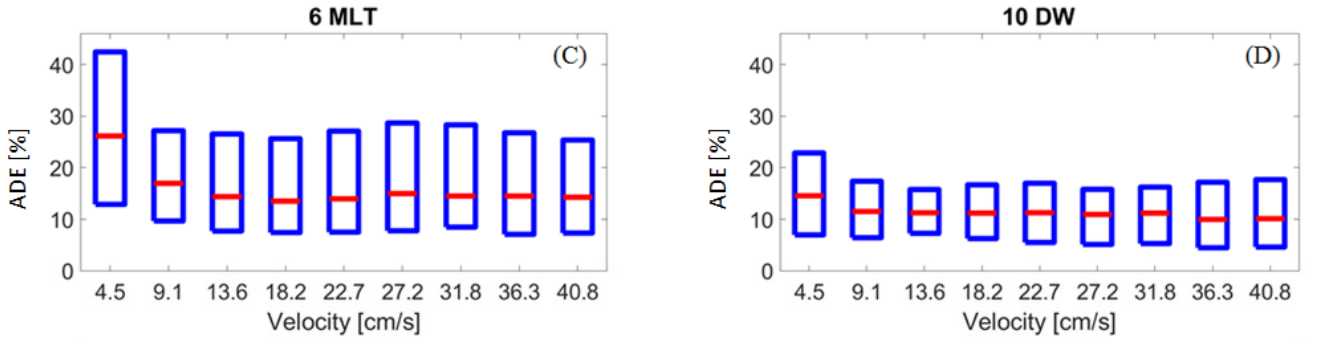

Velocity FR=450 Hz	4.5 cm/s	9.1 cm/s	13.6 cm/s	18.2 cm/s	22.7 cm/s	27.2 cm/s	31.8 cm/s	36.3 cm/s	40.8 cm/s	p-values for (Med_{MLT}, Med_{DW}) & (IQR_{MLT}, IQR_{DW})	Statistically different ($\alpha = 5 \cdot 10^{-2}$)
$Med_{MLT} - Med_{DW}$	11.58	5.45	3.13	2.32	2.69	4.04	3.29	4.51	4.15	$1.2 \cdot 10^{-3}$	yes
$IQR_{MLT} - IQR_{DW}$	13.65	6.55	10.32	7.77	8.08	10.21	8.86	6.97	4.94	$4.11 \cdot 10^{-5}$	yes

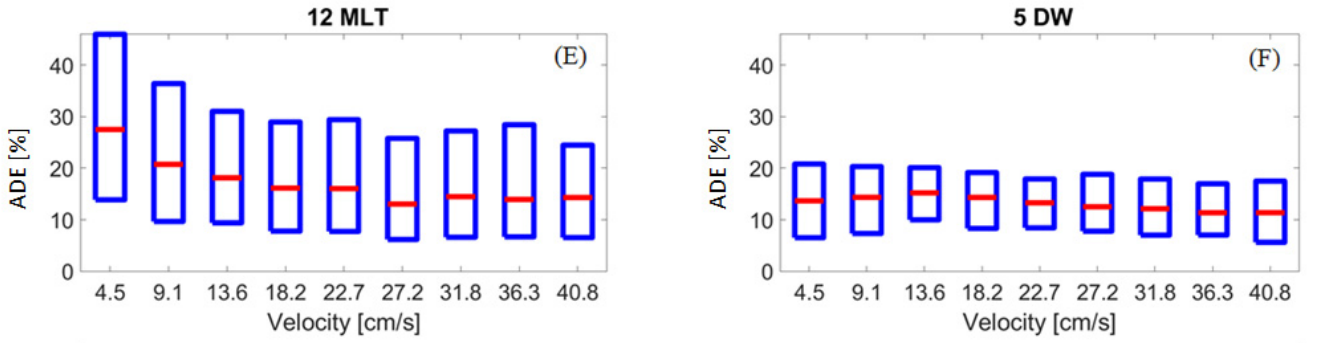

Velocity FR=900 Hz	4.5 cm/s	9.1 cm/s	13.6 cm/s	18.2 cm/s	22.7 cm/s	27.2 cm/s	31.8 cm/s	36.3 cm/s	40.8 cm/s	p-values for (Med_{MLT}, Med_{DW}) & (IQR_{MLT}, IQR_{DW})	Statistically different ($\alpha = 5 \cdot 10^{-2}$)
$Med_{MLT} - Med_{DW}$	13.82	6.38	2.92	1.8	2.76	0.52	2.33	2.57	2.94	$1.06 \cdot 10^{-2}$	yes
$IQR_{MLT} - IQR_{DW}$	17.78	13.72	11.48	10.30	12.18	8.56	9.72	11.78	6.05	$4.11 \cdot 10^{-5}$	yes

Fig. 5. *Lateral* (right) ADE at different velocities of the disc at different frame rates (*Speckle Tracking*): (a) and (b) 225 Hz, (c) and (d) 450 Hz, and (e) and (f) 900 Hz. Below each set of boxplot, we show the differences in median (*Med*) and IQR between MLT and DW. Additionally, we provide the associated *p*-values.

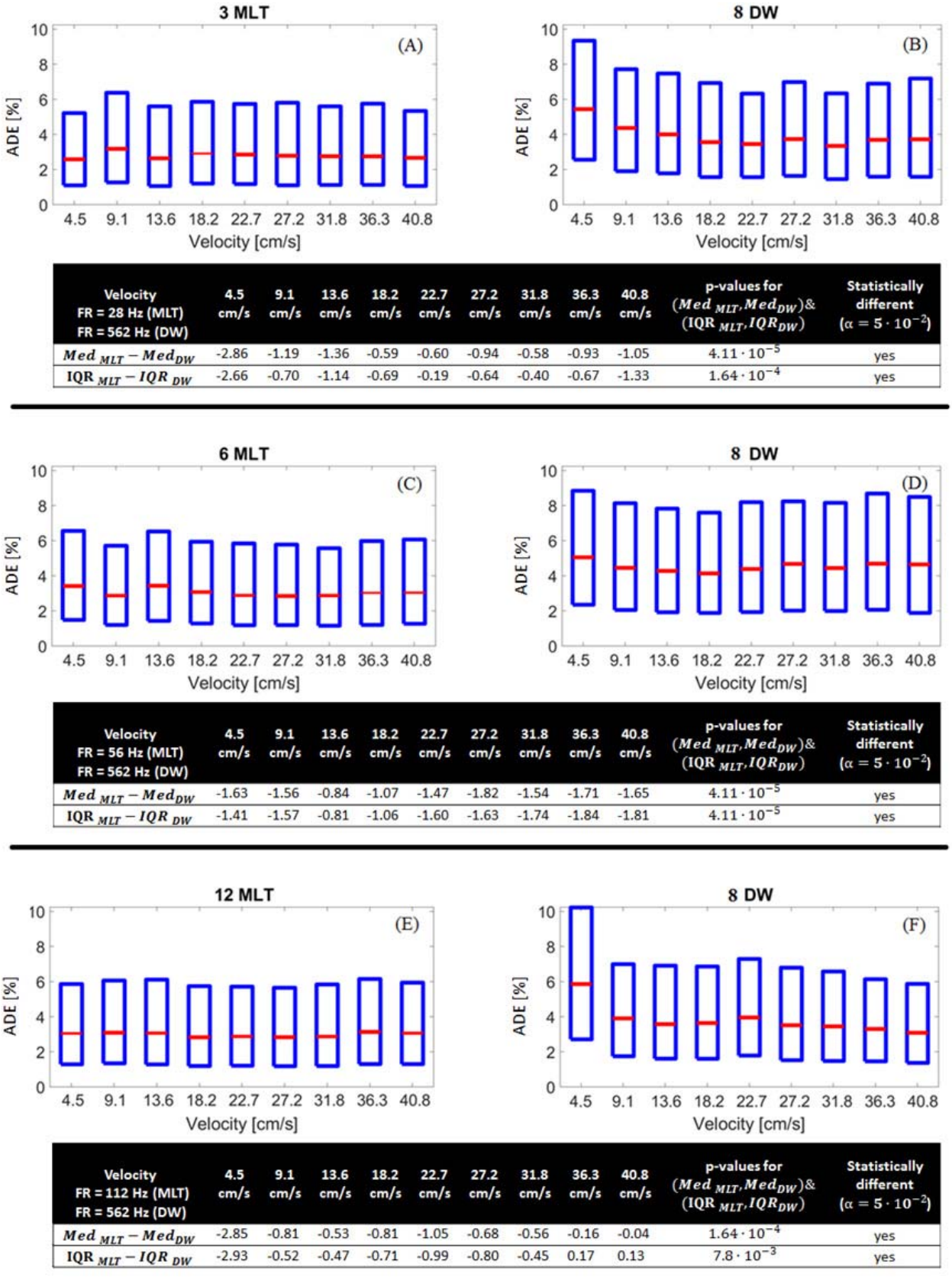

Velocity FR = 28 Hz (MLT) FR = 562 Hz (DW)	4.5 cm/s	9.1 cm/s	13.6 cm/s	18.2 cm/s	22.7 cm/s	27.2 cm/s	31.8 cm/s	36.3 cm/s	40.8 cm/s	p-values for (Med_{MLT}, Med_{DW})& (IQR_{MLT}, IQR_{DW})	Statistically different $(\alpha = 5 \cdot 10^{-2})$
$Med_{MLT} - Med_{DW}$	-2.86	-1.19	-1.36	-0.59	-0.60	-0.94	-0.58	-0.93	-1.05	$4.11 \cdot 10^{-5}$	yes
$IQR_{MLT} - IQR_{DW}$	-2.66	-0.70	-1.14	-0.69	-0.19	-0.64	-0.40	-0.67	-1.33	$1.64 \cdot 10^{-4}$	yes

Velocity FR = 56 Hz (MLT) FR = 562 Hz (DW)	4.5 cm/s	9.1 cm/s	13.6 cm/s	18.2 cm/s	22.7 cm/s	27.2 cm/s	31.8 cm/s	36.3 cm/s	40.8 cm/s	p-values for (Med_{MLT}, Med_{DW})& (IQR_{MLT}, IQR_{DW})	Statistically different $(\alpha = 5 \cdot 10^{-2})$
$Med_{MLT} - Med_{DW}$	-1.63	-1.56	-0.84	-1.07	-1.47	-1.82	-1.54	-1.71	-1.65	$4.11 \cdot 10^{-5}$	yes
$IQR_{MLT} - IQR_{DW}$	-1.41	-1.57	-0.81	-1.06	-1.60	-1.63	-1.74	-1.84	-1.81	$4.11 \cdot 10^{-5}$	yes

Velocity FR = 112 Hz (MLT) FR = 562 Hz (DW)	4.5 cm/s	9.1 cm/s	13.6 cm/s	18.2 cm/s	22.7 cm/s	27.2 cm/s	31.8 cm/s	36.3 cm/s	40.8 cm/s	p-values for (Med_{MLT}, Med_{DW})& (IQR_{MLT}, IQR_{DW})	Statistically different $(\alpha = 5 \cdot 10^{-2})$
$Med_{MLT} - Med_{DW}$	-2.85	-0.81	-0.53	-0.81	-1.05	-0.68	-0.56	-0.16	-0.04	$1.64 \cdot 10^{-4}$	yes
$IQR_{MLT} - IQR_{DW}$	-2.93	-0.52	-0.47	-0.71	-0.99	-0.80	-0.45	0.17	0.13	$7.8 \cdot 10^{-3}$	yes

Fig. 6. *Axial* ADE at different velocities of the disc (*Doppler*) by fixing the packet size to eight. The transmitted power was adjusted for DW to compare (a) with (b), (c) with (d), and (e) with (f). Below each set of boxplot, we show the differences in median (*Med*) and IQR between MLT and DW. Additionally, we provide the associated *p*-values.

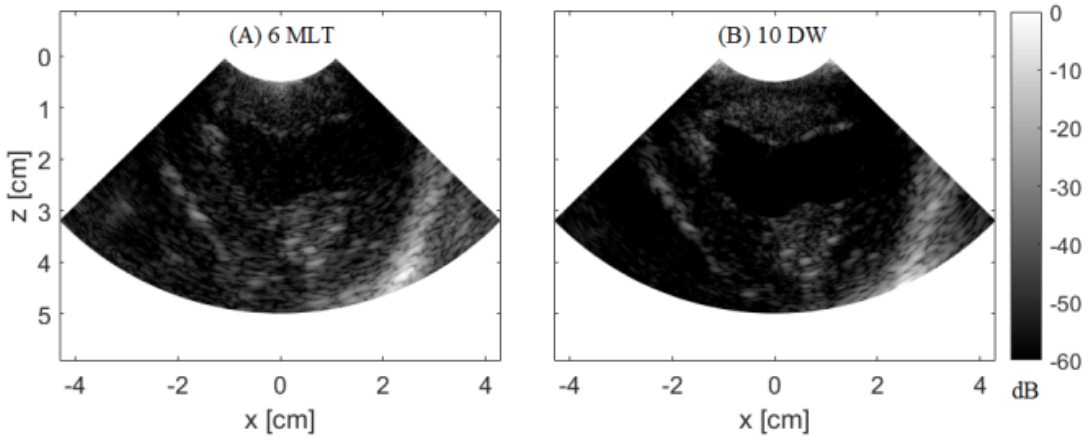

Fig. 7. B-mode *in vivo* images for (a) MLT and (b) DW at a frame rate of 450 Hz for the same phase of the cardiac cycle.

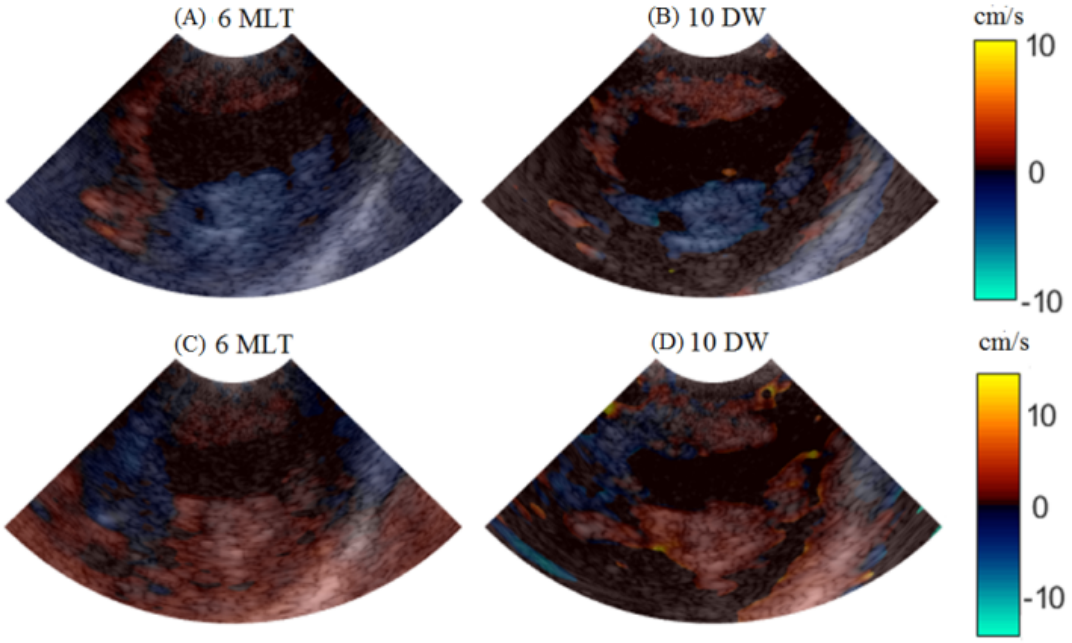

Fig. 8. TDI *in vivo* images for (a) and (c) MLT and (b) and (d) DW during two phases of the cardiac cycle: (a) and (b) when the mitral valve is fully opened and (c) and (d) when the mitral valve starts to close.

the Doppler frame rate is significantly limited as compared to a DW transmission. As shown in Table II, this leads to frame rates of 28, 56, and 112 Hz, depending on the amount of cross talks we would be ready to accept, as compared to a frame rate of 562 Hz with DW. Using a higher number of steering angles in DW may improve the Doppler estimates while providing a high enough frame rate, but increasing the packet size in MLT would reduce drastically the Doppler temporal resolution. For instance, using 32 steering angles for the first will result in a Doppler frame rate of 140 Hz, whereas using a 32-packet size for 3 MLT will result in a Doppler frame rate of 7 Hz. Additionally, an overlap of 50% can be used for the DW transmissions as suggested in [24], which would allow frame rates to be twice higher. If the two methods had been compared at the same Doppler frame rates, it is very likely that DW would have performed better than MLT. Using a higher number of transmissions for MoCo would have resulted in a better synthetic focusing. However, it would have been difficult to assess if the performance of the DW Doppler estimator had come from decreased variance (as a result of the packet size increase) or from the inherent features of the data obtained with the two imaging modalities (MLT and DW).

By increasing the number of cycles from 1 and 1.5 cycles in TDI (to balance the total power from 6 MLT to 3 MLT configurations), the TDI accuracy is influenced. For instance, we can observe a slight difference in the median ADE between Fig. 6(b) and (d), which on average (over all velocities) is 13%.

A possible improvement of the TDI estimator for both methods could have been achieved by using even longer transmission pulses (more cycles). However, due to hardware constraints, we could not increase the duration of the transmitted MLT signal and we needed to balance the DW transmission signal accordingly [(3) and (4)]. It is also worth mentioning that balancing the total power of the transmitted

waveforms does not guarantee the same acoustic power for the two methods, which could be an alternative to our acquisition settings.

C. In Vivo Acquisitions

B-mode *in vivo* acquisitions showed that the two methods are competitive in providing good image quality at high frame rates (Fig. 7). However, the presence of crosstalk next to the surface of the probe in MLT makes DW a better candidate for the visualization of low depth structures. This could explain the cluttered appearance of MLT images. The presence of these artifacts in the region of interest could be reduced by placing a gel pad between the probe and the surface of the heart. As also demonstrated *in vitro*, the contrast up to 4 cm is better with DW than with MLT. TDI images illustrated in Fig. 8 demonstrate competitive performances of the two methods in providing good qualitative velocity estimates.

D. Overall Results and Limitations

Overall, the obtained results show that the choice of using one ultrafast method over the other depends on the application. Even if for the B-Mode visualization of organs placed at a lower depth, DW is more adapted than MLT, the energy dissipates faster with the penetration depth compared to MLT. Although cardiac images are characterized by rapid movements, the CNR seems to be better preserved with MLT. Competitive speckle tracking estimates were found for the two methods in the axial direction, while the error was significantly higher for MLT in the lateral direction. In terms of Doppler velocity estimator, MLT provides slightly lower errors than DW, but much higher Doppler frame rates can be obtained with DW. Even if MLT may be enough for TDI, higher frame rates may be desirable for the blood velocity estimation case, in which DW would be more adapted. Since the MLT Doppler temporal resolution is considerably affected if a full image needs to be reconstructed, estimating the velocity just over a few lines of interest in the image would definitely eliminate this limitation.

It is important to highlight that our overall results are valid for our specific acquisition settings that were fixed to provide similar conditions for the two methods (same transmitted power, frame rate for image quality and STE, and same packet size for TDI). An interesting alternative to our choice would have been to optimize each method. Using coded excitations could have been an interesting approach. Due to hardware constraints, we could not use a longer pulse for MLT and we adapted the transmitted signal for DW accordingly. Moreover, comparing the two methods at the same frame rate for TDI would have resulted in superior performances of DWI.

V. Conclusion

In this study, we compared two ultrafast methods under static and dynamic conditions for *in vitro* and *in vivo* experiments. Since both methods can provide competitive frame rates compared to conventional imaging, our aim was to evaluate their performance at different frame rates, superior to the ones specific for SLT. We were particularly interested in analyzing the image quality and in assessing the influence of each ultrafast method on two motion estimation techniques commonly used in echocardiography: speckle tracking and TDI.

The performance of the two ultrafast competitive methods was investigated for different frame rates and different velocities. DWI provides better image quality at limited depths, whereas MLT imaging allows a better concentration of the energy around a focal point that could be placed at higher depths. Similar speckle tracking axial errors were obtained for the two methods, but DW with MoCo provides better lateral estimates than MLT. Slightly lower TDI errors were obtained for MLT, but much higher Doppler frame rates can be obtained with DW.

The two methods were shown to be competitive in both image quality and motion estimation, and the choice for a certain method is dependent on the application.

For example, DWI is more suitable for color Doppler applications due to the high frame rate that could be achieved by using this imaging method. Also, imaging structures at low depths at good image quality and without any particular artifacts (as it would be the case for MLT) can definitively be obtained with DW. On the other hand, MLT can provide very good image quality close to the focal point (that could be placed at higher depths) and time-resolved velocities along different lines of the image (corresponding to simultaneous transmissions).

Acknowledgment

This work was performed within the framework of the LABEX PRIMES (ANR-11-LABX-0063) of the Université de Lyon, within the program "Investissements d'Avenir" (ANR-11-IDEX-0007) operated by the French National Research Agency (ANR).

The Verasonics system was cofounded by the FEDER Program, Saint-EtienneMetropole (SME), and Conseil General de la Loire (CG42) within the framework of the SonoCardio-Protection Project led by Dr. P. Croisille.

References

[1] M. Cikes, L. Tong, G. R. Sutherland, and J. D'hooge, "Ultrafast cardiac ultrasound imaging: Technical principles, applications, and clinical benefits," *JACC, Cardiovascular Imag.*, vol. 7, no. 8, pp. 812–823, Aug. 2014.

[2] C. Bruneel, R. Torguet, K. M. Rouvaen, E. Bridoux, and B. Nongaillard, "Ultrafast echotomographic system using optical processing of ultrasonic signals," *Appl. Phys. Lett.*, vol. 30, no. 8, pp. 371–373, Apr. 1977.

[3] D. P. Shattuck, M. D. Weinshenker, S. W. Smith, and O. T. von Ramm, "Explososcan: A parallel processing technique for high speed ultrasound imaging with linear phased arrays," *J. Acoust. Soc. Amer.*, vol. 75, no. 4, pp. 1273–1282, 1984.

[4] M. Fink, "Time reversal of ultrasonic fields. I. Basic principles," *IEEE Trans. Ultrason., Ferroelectr., Freq. Control*, vol. 39, no. 5, pp. 555–566, Sep. 1992.

[5] S. Wang, W.-N. Lee, J. Provost, J. Luo, and E. E. Konofagou, "A composite high-frame-rate system for clinical cardiovascular imaging," *IEEE Trans. Ultrason., Ferroelectr., Freq. Control*, vol. 55, no. 10, pp. 2221–2233, Oct. 2008.

[6] M. Karaman, P.-C. Li, and M. O'Donnell, "Synthetic aperture imaging for small scale systems," *IEEE Trans. Ultrason., Ferroelectr., Freq. Control*, vol. 42, no. 3, pp. 429–442, May 1995.

[7] L. Sandrin, S. Catheline, M. Tanter, X. Hennequin, and M. Fink, "Time-resolved pulsed elastography with ultrafast ultrasonic imaging," *Ultrason. Imag.*, vol. 21, no. 4, pp. 259–272, Oct. 1999.

[8] H. Hasegawa and H. Kanai, "High-frame-rate echocardiography using diverging transmit beams and parallel receive beamforming," *J. Med. Ultrason.*, vol. 38, no. 3, pp. 129–140, 2011.

[9] R. Mallart and M. Fink, "Improved imaging rate through simultaneous transmission of several ultrasound beams," *Proc. SPIE*, vol. 1733, 1992, pp. 120–130.

[10] J. Provost, W.-N. Lee, K. Fujikura, and E. E. Konofagou, "Electromechanical wave imaging of normal and ischemic hearts *in vivo*," *IEEE Trans. Med. Imag.*, vol. 29, no. 3, pp. 625–635, Mar. 2010.

[11] S. I. Nikolov and J. A. Jensen, "*In-vivo* synthetic aperture flow imaging in medical ultrasound," *IEEE Trans. Ultrason., Ferroelectr., Freq. Control*, vol. 50, no. 7, pp. 848–856, Jul. 2003.

[12] C. Papadacci, M. Pernot, M. Couade, M. Fink, and M. Tanter, "High-contrast ultrafast imaging of the heart," *IEEE Trans. Ultrason., Ferroelectr., Freq. Control*, vol. 61, no. 2, pp. 288–301, Feb. 2014.

[13] J. Faurie *et al.*, "Intracardiac vortex dynamics by high-frame-rate Doppler vortography—*in vivo* comparison with vector flow mapping and 4-D flow mri," *IEEE Trans. Ultrason., Ferroelectr., Freq. Control*, vol. 64, no. 2, pp. 424–432, Feb. 2017.

[14] L. Tong, H. Gao, and J. D'hooge, "Multi-transmit beam forming for fast cardiac imaging-a simulation study," *IEEE Trans. Ultrason., Ferroelectr., Freq. Control*, vol. 60, no. 8, pp. 1719–1731, Aug. 2013.

[15] L. Tong, A. Ramalli, R. Jasaityte, P. Tortoli, and J. D'hooge, "Multi-transmit beam forming for fast cardiac imaging—Experimental validation and *in Vivo* application," *IEEE Trans. Med. Imag.*, vol. 33, no. 6, pp. 1205–1219, Jun. 2014.

[16] L. Demi, M. D. Verweij, and K. W. A. Van Dongen, "Parallel transmit beamforming using orthogonal frequency division multiplexing applied to harmonic imaging-a feasibility study," *IEEE Trans. Ultrason., Ferroelectr., Freq. Control*, vol. 59, no. 11, pp. 2439–2447, Nov. 2012.

[17] A. Rabinovich, A. Feuer, and Z. Friedman, "Multi-line transmission combined with minimum variance beamforming in medical ultrasound imaging," *IEEE Trans. Ultrason., Ferroelectr., Freq. Control*, vol. 62, no. 5, pp. 814–827, May 2015.

[18] L. Tong *et al.*, "Wide-angle tissue Doppler imaging at high frame rate using multi-line transmit beamforming: An experimental validation *in vivo*," *IEEE Trans. Med. Imag.*, vol. 35, no. 2, pp. 521–528, Feb. 2016.

[19] A. Ramalli *et al.*, "Real-time high-frame-rate cardiac B-mode and tissue Doppler imaging based on multiline transmission and multiline acquisition," *IEEE Trans. Ultrason., Ferroelectr., Freq. Control*, vol. 65, no. 11, pp. 2030–2041, Nov. 2018.

[20] G. Montaldo, M. Tanter, J. Bercoff, N. Benech, and M. Fink, "Coherent plane-wave compounding for very high frame rate ultrasonography and transient elastography," *IEEE Trans. Ultrason., Ferroelectr., Freq. Control*, vol. 56, no. 3, pp. 489–506, Mar. 2009.

[21] G. E. Trahey and L. P. Nock, "Synthetic receive aperture imaging with phase correction for motion and for tissue inhomogeneities. II. Effects of and correction for motion," *IEEE Trans. Ultrason., Ferroelectr., Freq. Control*, vol. 39, no. 4, pp. 496–501, Jul. 1992.

[22] B. Denarie *et al.*, "Coherent plane wave compounding for very high frame rate ultrasonography of rapidly moving targets," *IEEE Trans. Med. Imag.*, vol. 32, no. 7, pp. 1265–1276, Jul. 2013.

[23] K. L. Gammelmark and J. A. Jensen, "2-D tissue motion compensation of synthetic transmit aperture images," *IEEE Trans. Ultrason., Ferroelectr., Freq. Control*, vol. 61, no. 4, pp. 594–610, Apr. 2014.

[24] J. Porée, D. Posada, A. Hodzic, F. Tournoux, G. Cloutier, and D. Garcia, "High-frame-rate echocardiography using coherent compounding with Doppler-based motion-compensation," *IEEE Trans. Med. Imag.*, vol. 35, no. 7, pp. 1647–1657, Jul. 2016.

[25] P. Joos *et al.*, "High-frame-rate speckle-tracking echocardiography," *IEEE Trans. Ultrason., Ferroelectr., Freq. Control*, vol. 65, no. 5, pp. 720–728, May 2018.

[26] J. Porée, M. Baudet, F. Tournoux, G. Cloutier, and D. Garcia, "A dual tissue-Doppler optical-flow method for speckle tracking echocardiography at high frame rate," *IEEE Trans. Med. Imag.*, vol. 37, no. 9, pp. 2022–2032, Sep. 2018.

[27] H. Liebgott, A. Rodriguez-Molares, F. Cervenansky, J. A. Jensen, and O. Bernard, "Plane-wave imaging challenge in medical ultrasound," in *Proc. IEEE Int. Ultrason. Symp. (IUS)*, Sep. 2016, pp. 1–4.

[28] I. A. Hein and W. D. O'Brien, "Current time-domain methods for assessing tissue motion by analysis from reflected ultrasound echoes-a review," *IEEE Trans. Ultrason., Ferroelectr., Freq. Control*, vol. 40, no. 2, pp. 84–102, Mar. 1993.

[29] C. Kasai, K. Namekawa, A. Koyano, and R. Omoto, "Real-time two-dimensional blood flow imaging using an autocorrelation technique," *IEEE Trans. Sonics Ultrason.*, vol. 32, no. 3, pp. 458–464, May 1985.

[30] T. Loupas, J. T. Powers, and R. W. Gill, "An axial velocity estimator for ultrasound blood flow imaging, based on a full evaluation of the Doppler equation by means of a two-dimensional autocorrelation approach," *IEEE Trans. Ultrason., Ferroelectr., Freq. Control*, vol. 42, no. 4, pp. 672–688, Jul. 1995.

[31] M. Zhang *et al.*, "Extension of Fourier-based techniques for ultrafast imaging in ultrasound with diverging waves," *IEEE Trans. Ultrason., Ferroelectr., Freq. Control*, vol. 63, no. 12, pp. 2125–2137, Dec. 2016.